Co-expression of calcium channels and delayed rectifier potassium channels protects the heart from proarrhythmic events

Sara Ballouz[a,1], Melissa M Mangala[b,1], Matthew D Perry[b,c,1], Stewart Heitmann[b], Jesse A Gillis[a], Adam P Hill[b,c,2], Jamie I Vandenberg[b,c,2]

Author Affiliation:

a. Stanley Institute for Cognitive Genomics, Cold Spring Harbor Laboratory, Woodbury, NY 11797, USA.
b. Victor Chang Cardiac Research Institute, Darlinghurst, NSW 2010, Australia
c. University of NSW, Sydney. Kensington, NSW 2052, Australia

1. These authors contributed equally to this study

2. Corresponding Authors:

Jamie I Vandenberg* and Adam P Hill†,
Victor Chang Cardiac Research Institute,
Lowy Packer Building, 405 Liverpool Street
Darlinghurst, NSW 2010
Australia

* j.vandenberg@victorchang.edu.au
† a.hill@victorchang.edu.au

Abstract (147 words)

Cardiac electrical activity is controlled by the carefully orchestrated activity of more than a dozen different ion conductances. Yet, there is considerable variability in cardiac ion channel expression levels both within and between subjects. In this study we tested the hypothesis that variations in ion channel expression between individuals are not random but rather there are modules of co-expressed genes and that these modules make electrical signaling in the heart more robust.

Meta-analysis of 3653 public RNA-Seq datasets identified a strong correlation between expression of *CACNA1C* (L-type calcium current, I_{CaL}) and *KCNH2* (rapid delayed rectifier K^+ current, I_{Kr}), which was verified in mRNA extracted from human induced pluripotent stem cell-derived cardiomyocytes (hiPSC-CM). *In silico* modeling, validated with functional measurements in hiPSC-CM, indicates that the co-expression of *CACNA1C* and *KCNH2* limits the variability in action potential duration and reduces susceptibility to early afterdepolarizations, a surrogate marker for pro-arrhythmia.

Keywords:

Ion channels; calcium channels, potassium channels, co-expression; gene modules; meta-analysis; cardiac action potential, early afterdepolarization, arrhythmia, drug-induced long QT syndrome,

Impact Statement

Coexpressed levels of potassium and calcium ion channel genes in the heart encode more robust cardiac electrophysiology and provide insights into genetic basis of arrhythmic risk

Introduction

Robust electrical signaling in the heart is critical for co-ordinating the efficient pumping of blood around the body. Failure of cardiac electrical signaling, even for just a few minutes, can have fatal consequences, with sudden cardiac death accounting for up to 10% of deaths in our community (1). Despite decades of research, predicting in advance who is more or less susceptible to sudden cardiac death remains challenging (2).

The action potential (AP) of excitable cells, such as cardiac myocytes and neurons, reflects the orchestrated activity of at least a dozen distinct ion channels and electrogenic transporters (3,4). In such complex systems, both theoretical and experimental studies have shown that there is considerable inter-individual variability in the combinations of molecular input parameters that can produce very similar integrated outputs (5,6). This has led to a paradigm shift in computational cardiology that relies not on generating idealized outputs based on mean data but rather development of populations of models that account for the observed variability in molecular inputs (7,8). Such models are already proving useful for interrogating inter-individual variability in response to pathological stimuli (9-11). Our challenge now is to discern the underlying essence of these complex systems (12,13) so that we may then make rational interventions to treat pathology that takes into account inter-individual variation. Specifically, are there underlying principles regulating cardiac electrical activity that can provide insights into why some people are more susceptible to sudden cardiac death in response to pathological stimuli, such as drug block of the rapid delayed rectifier potassium channel (I_{Kr}) which is the underlying basis of drug-induced long QT syndrome (di-LQTS) (14).

A common approach to discern patterns in multi-dimensional biological problems has been to look for co-expression networks (13,15). Co-expression networks are known to encode functional information (16), with co-expression reflecting co-regulation and co-functionality (17,18). To help identify robust co-expression modules, it is helpful to use meta-analytical approaches, which aggregate large numbers of individual networks across multiple independent experiments to average away noise and reinforces those correlations that reflect real signals (19-21).

86 Here, we have used meta-analytic co-expression analysis in large scale human gene
87 expression data sets to identify modules of co-expressed ion channel genes which were
88 then used to constrain population models of cardiac electrical activity. These models were
89 then used to test the hypothesis that co-expression of repolarization and depolarization
90 currents helps prevent irregular APs in human cardiac myocytes that are exposed to pro-
91 arrhythmic stimuli. We show that tight coupling of current densities for the L-type calcium
92 current (I_{CaL}) and the rapid component of the delayed rectifier potassium current (I_{Kr})
93 reduced the emergence of pro-arrhythmic early afterdepolarizations (EADs) and this
94 protection persisted in the face of highly variable expression of other ion channels, as well
95 as in the presence of pharmacological block of I_{Kr} which is a potent pro-arrhythmic
96 stimulus (22). A very important prediction to arise out of our modelling studies is that in
97 the context of drug block of I_{Kr}, those patients with low expression of I_{CaL} and I_{Kr} will
98 exhibit the greatest prolongation of repolarization duration but patients with high
99 expression of I_{CaL} and I_{Kr} will experience more EADs and are therefore more likely to be
100 susceptible to ventricular arrhythmias.

101

102

103 **Results**

104 The shape and duration of action potentials in cardiac myocytes are determined by the
105 orchestrated activity of voltage-gated sodium, calcium and potassium channels, as well as
106 a series of electrogenic transporters that regulate intracellular ion concentrations. These
107 channels, transporters and related intracellular calcium handling proteins are encoded by
108 a few dozen genes, sometimes referred to as the rhythmonome (23) (a full list is provided
109 in **Figure 1 source data 1**).

110 To determine whether there were any co-expression patterns among the rhythmonome
111 genes we first undertook an untargeted screen for possible expression correlation
112 patterns in publicly available RNA-seq data sets (**Figure 1**). Ranked correlation
113 coefficients from an aggregate co-expression network that contain data from 3653
114 samples are illustrated in the heatmap in **Figure 1A**. High ranked correlations indicate

similarity of transcriptional profiles between the genes. A clustering analysis, as shown by the dendrogram in **Figure 1A**, groups genes according to their correlation similarities, as defined by the Spearman's correlation coefficients (see color code in **Figure 1A**). There is a large cluster of yellow/green squares in the bottom left corner indicating that there are significant levels of correlation amongst many of the genes. Furthermore, within this large cluster there are two sub-clusters. The cluster of yellow-green squares corresponding to 13 genes in the bottom left corner (red dashed box in **Figure 1A**) encode for proteins that regulate calcium fluxes as well as the transient outward K^+ current (*KCND3*), which helps to maintain the plateau potential at a level that maximizes calcium influx (24). A second sub-cluster, in the upper right quadrant of the main cluster, encompasses 10 genes (black dashed box in **Figure 1A),** including *KCNH2, SCN5A, KCNJ12* and *KCNIP2*, that encode for ion channel proteins important for regulating action potential duration (APD).

Figure 1: Cardiac ion channel and calcium handling protein co-expression connectivity analysis from published RNA-seq datasets

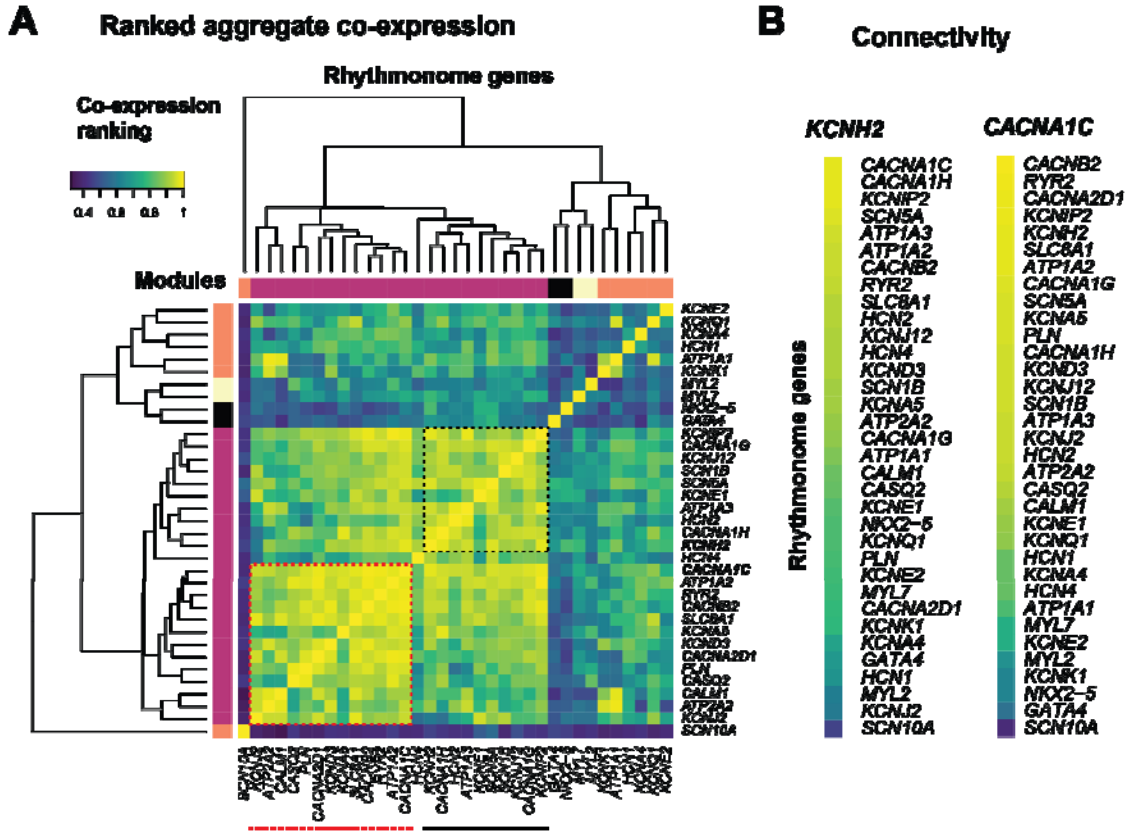

The full list of RNA-seq experiments interrogated are summarized in **Figure 1 source data 1**). **A.** Sub-network of co-expression ranking across 35 genes encoding for cardiac ion channels or calcium homeostasis proteins. Blue: low ranked correlations, yellow: high ranked correlations. The dendrogram illustrates the modules of genes with high levels of similarity in their transcriptional profiles. Red and black dashed boxes highlight subnetworks of correlated genes **B**. Connectivity of genes to *KCNH2* (encodes for I_{Kr}) and *CACNA1C* (encodes for I_{CaL}).

Figure 1 - figure supplement 1: Network connectivity for each rhythmonome gene

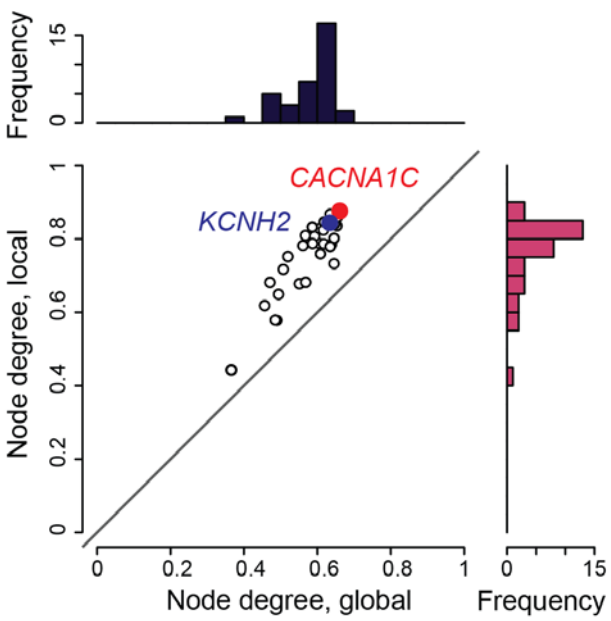

Network connectivity for each rhythmonome gene within the local rhythmonome network (y-axis) versus its connectivity within the whole genome (x-axis). All the rhythmonome genes are more highly connected within the local network (i.e., all the points lie above the line of identity, $p \sim 5.7e^{-14}$). *CACNA1C* is highlighted in red and *KCNH2* in blue.

Overall, the connectivity within the set of rhythmonome genes is fairly high in comparison to their connectivity to all other genes in the co-expression network (node degree analysis, p~5.7e-14), with a central gene being *CACNA1C*, the gene encoding the alpha subunit of the L-type calcium channel (see **Figure 1, figure supplement 1**). Although *CACNA1C* clusters in the group of calcium handling genes in the bottom left quadrant of the main cluster in **Figure 1A**, it also shows high correlation with the cluster of ion channel genes in the top right quadrant of **Figure 1A**. In a similar fashion, the *KCNH2* gene, which encodes for I_{Kr}, is included in the ion channel cluster but also shows moderate-high correlations with a portion of the calcium handling genes in the bottom left quadrant. The highest ranked co-expression partners for *CACNA1C* and *KCNH2* are highlighted in **Figure 1B**.

173 The vast majority of the public RNA-Seq datasets included in our analyses were not heart
174 specific. It is, however, noteworthy that there are no strong correlations between the
175 expression of any of the individual ion channel or calcium handling genes and the cardiac-
176 specific markers included in our analyses: *GATA-4*, *NKX2-5*, *MYL2* and *MYL7*. For example,
177 the cardiac marker genes are towards the bottom of the lists in **Figure 1B**. This suggests
178 that the correlations within the set of rhythmonome genes are not simply a reflection of
179 cardiac specific expression but rather represent intrinsic correlations.

180 To investigate whether the meta-analytic co-expression patterns observed in **Figure 1**
181 were also seen in human heart cells, we extracted mRNA from human induced pluripotent
182 stem cell-derived cardiomyocytes (hiPSC-CMs) (25) obtained from 10 patients with no
183 known heart disease. All samples contained high levels of cardiac marker genes (*MYL7,*
184 *GATA4* and *NKX2*.5) **(Figure 2A)**. The levels of expression of most rhythmonome genes
185 showed variations between the samples that spanned approximately an order of
186 magnitude. However, similar to the generic tissue RNA-Seq datasets, there were modules
187 of co-expressed genes (e.g., see dashed box in bottom left quadrant of **Figure 2B**). Most of
188 the 13 genes in the cluster in **Figure 2B** are present in the modules highlighted by the
189 black and red dashed boxes in **Figure 1A**. Conversely, many of the ion channel genes
190 contained in the modules highlighted in **Figure 1** are not present in the module in **Figure**
191 **2** (e.g. *KCNJ2/KCNJ12*, which encodes for I_{K1}; *KCND3*, which encodes for I_{To}; and *SCN5A*,
192 which encodes for I_{Na}). These genes are all known to be expressed at lower levels in
193 embryonic hearts and so it is unsurprising that they are not well expressed in the hiPSC-
194 CM lines (26).

195 We next looked to see if there were any specific relationships between genes encoding
196 depolarization and repolarization currents, within the hiPSC-CM expression profiles. In
197 **Figure 2C,** we have plotted the expression of *KCNH2* versus the genes that encode for the
198 depolarization currents that showed the highest levels of correlation with expression of
199 *KCNH2* in the generic tissue datasets (see **Figure 1B**, i.e., *CACNA1C*, *CACNA1H* and *SCN5A*).
200 The most notable correlation that was observed in the hiPSC-CMs was that between
201 *KCNH2* and *CACNA1C*; $r^2 = 0.68$ (**Figure 2C**).

202

Figure 2: HiPSC-CM mRNA correlation analysis

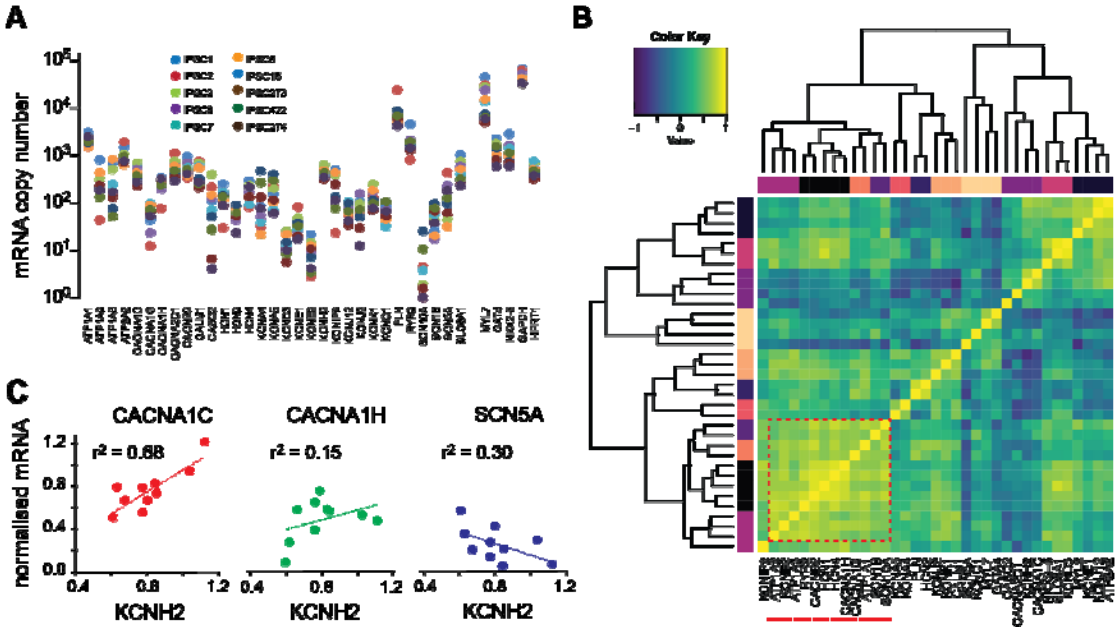

A. plot of all mRNAs (log axis) for 10 hiPSC-CM lines. Note that there are high levels of expression of cardiac markers (*MYL7* as well as *NKX2-5* and *GATA4*) in all cell lines. Also, there is less variability in the levels for the housekeeping genes (*GAPDH* and *HPRT1*) compared to that seen for the ion channels and calcium handling proteins. The mRNA data for panel A are provided in Figure 2 -Source Data 1 (GEO: TBA). **B.** Correlation matrix for hiPSC-CM mRNA. The red dashed box highlights the module with the highest correlations. **C.** Correlation plots for normalised mRNA expression *KCNH2* versus genes that encode the major depolarizing currents (*CACNA1C*, *CACNA1H* and *SCN5A*). To account for any differences in mRNA loading between runs, levels of expression have been normalized to GAPDH.

As the most robust relationship that we observed in both the generic tissue sets and the hiPSC-CM lines was the co-expression of *KCNH2* and *CACNA1C*, we focused on this pair for our subsequent studies. To investigate whether co-expression modules of ion channel genes might influence integrated cardiac electrical function, we used an *in silico* approach (**Figure 3**). We used the O-Hara-Rudy model of the human ventricular myocyte (27) with the baseline conductance scalars optimized as previously described (28). First, we simulated a population of 1000 human cardiac APs where the ion conductances for each cell were scaled randomly (see **Figure 3A**. **Figure 3 movie supplement 1**).

Figure 3: *In silico* predictions of conductance scalars that give APD_{90} values in the normal range

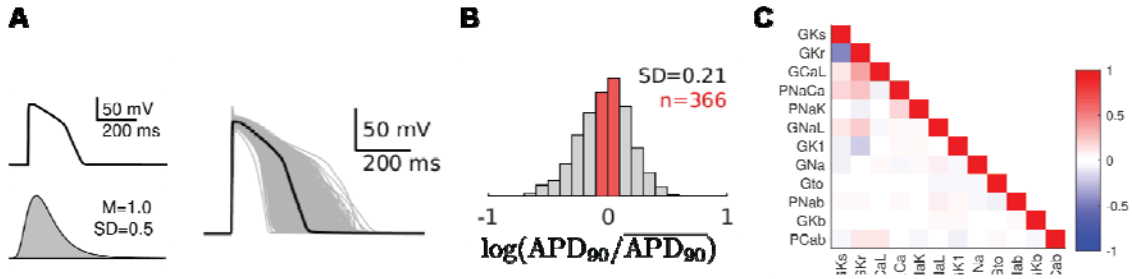

A. Baseline AP model and frequency histogram of scalars (log normal distribution with a mean of 1 and SD of 0.5) used to generate the population of 1000 APs with the baseline AP (all scalars set to 1.0) shown in black. The last 4 beats for each of the population of 1000 APs are shown in the **Figure 3 movie supplement 1** (see below). **B.** Frequency histogram of APD_{90} values for the 1000 simulations with those falling within ±20% of the mean value shown in red. **C.** correlation matrix for sets of conductance scalars that gave APD_{90} values within ±20% of the mean value

Figure 3 Movie supplement 1: Last 4 beats for the population of 1000 simulated APs

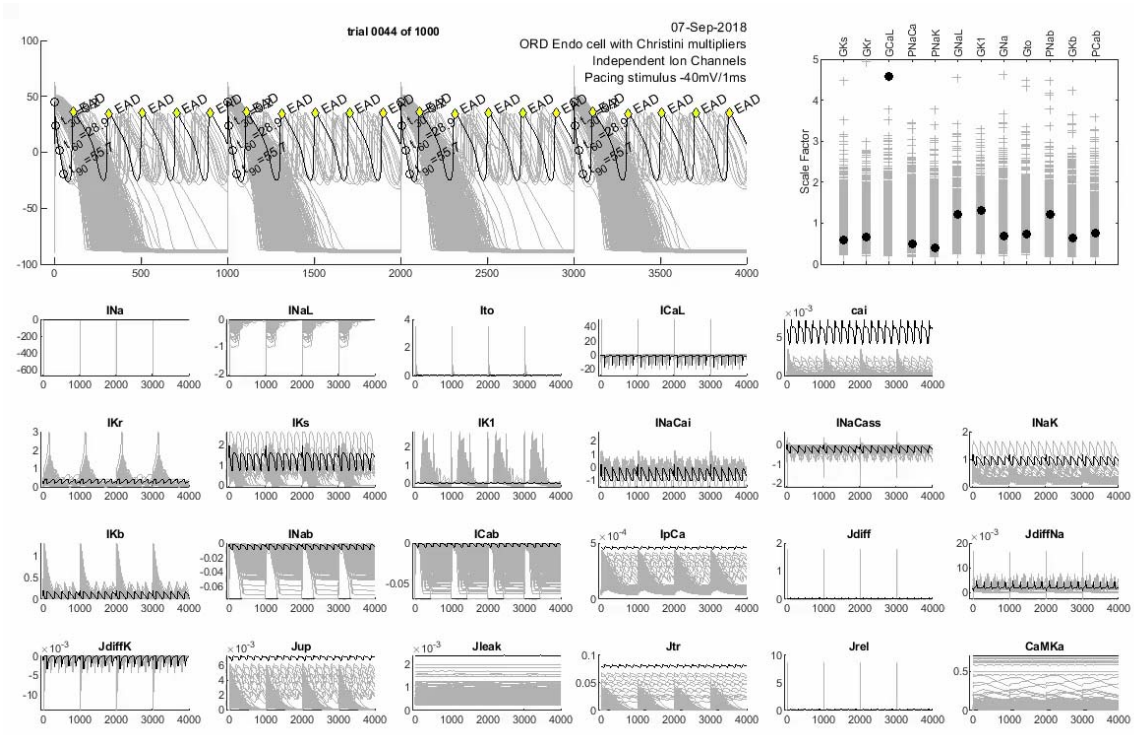

The baseline action potential produced by this model (black trace in right hand panel of **Figure 3A**) has a duration at the point of 90% repolarization (APD_{90}) of 264 ms. Whereas, the APD_{90} values in the cells with randomized conductance scalars ranged from ~120 ms

to ~500 ms (**Figure 3A,** right panel). We next selected those cells with APD_{90} values that fell within 20% of the mean value (red bars, **Figure 3B**) to determine if there were any patterns of ion channel co-expression that could contribute to keeping the APD_{90} within this narrow-selected range. The correlation matrix of the conductance scaling factors for the selected cells (**Figure 3C**) reveals a positive correlation between G_{Kr} and G_{CaL} (R=0.36) as well as an inverse correlation for G_{Kr} and G_{Ks} (R=-0.46). The positive correlation between the conductance scalars G_{Kr} and G_{CaL} in the *in silico* modelling dataset (**Figure 3**) suggests that the correlation seen between *CACNA1C* and *KCNH2* mRNA expression in both the public RNA-Seq datasets (**Figure 1**) and the hiPSC-CM dataset (**Figure 2**) would contribute to reducing the population variability in APD_{90} values.

We next repeated our previous simulation but forced the conductance scaling factors for I_{Kr} and I_{CaL} to be identical in each cell (denoted co-expression in **Figure 4**). The scaling factors for all other conductances were allowed to vary independently. The distribution of

Figure 4: Impact of I_{Kr}-I_{CaL} co-expression and conductance scalar variability on APD_{90} variability

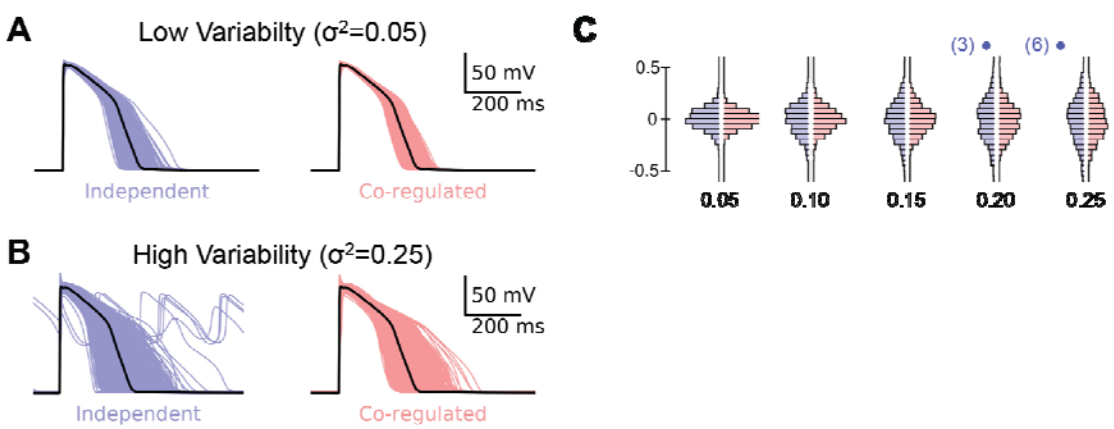

APs for independent (blue) and co-expression of G_{Kr}-G_{CaL} (red) for **A.** low scalar variability (σ^2=0.05) and **B.** high scalar variability (σ^2=0.25). Note the presence of EADs in 6 of the APs in the independent group with σ^2 = 0.25. The last 4 beats for each of the population of 1000 APs are shown in the **Figure 4 movie supplement 1**. **C.** Histograms of log(APD_{90}/mean APD_{90}) distributions for co-expressed (red) or independent (blue) G_{Kr}-G_{CaL} simulations with σ^2 = 0.05, 0.1, 0.15, 0.2, 0.25. The numbers in parentheses above the 0.2 and 0.25 groups indicate the number of EADs in each independent scalars group. APs and incidence of EADs for an extended range of variances are shown in **Figure 4 figure supplement 1**.

Figure 4 figure supplement 1: Population models of ventricular APs with different levels of scalar variance

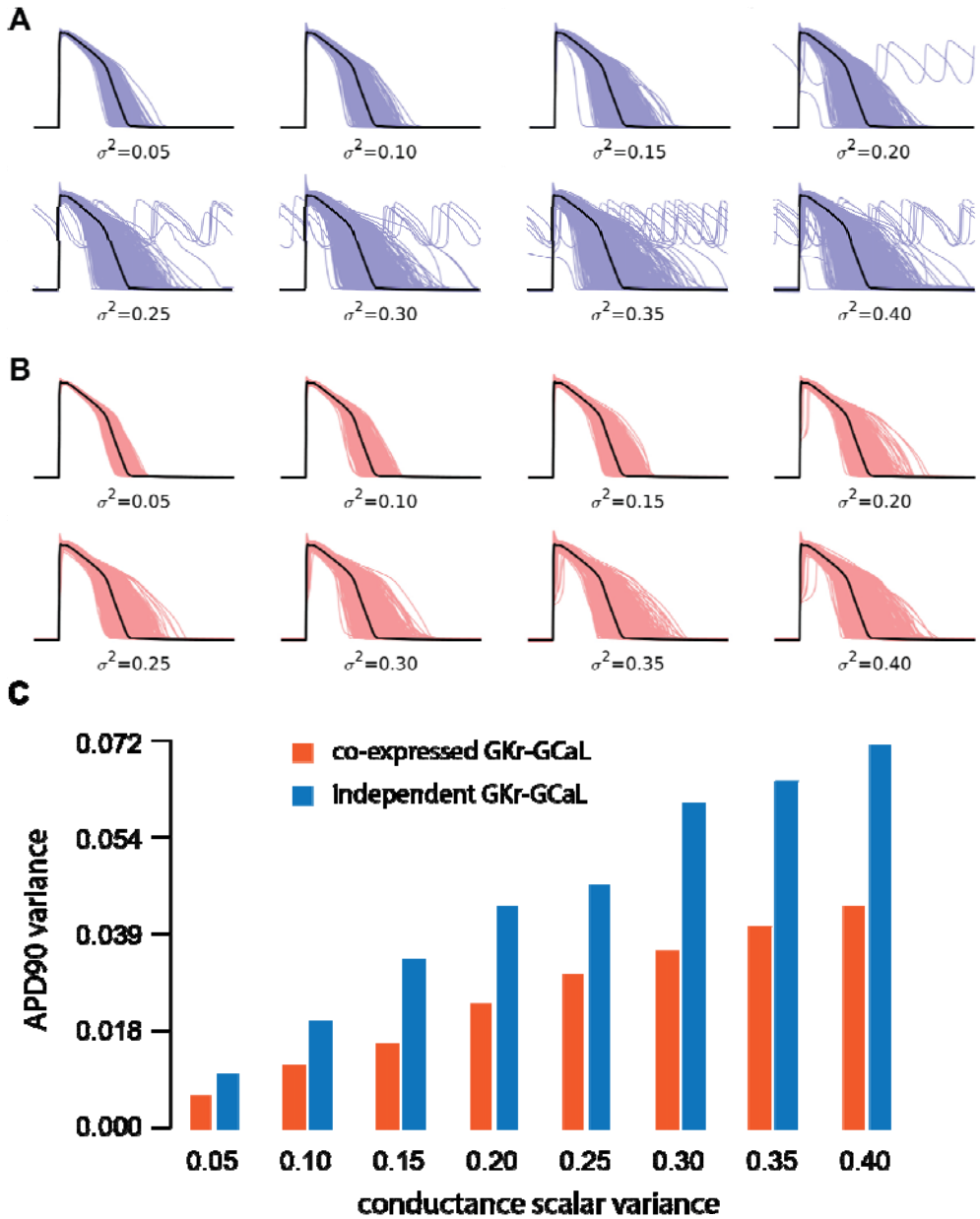

A-B. Population of models with variance systematically increased from σ2 = 0.05 to 0.40 for independent conductance scalars for G_{Kr} and G_{CaL} **(A),** or co-expression conductance scalars for G_{Kr} and G_{CaL} **(B)**. As the variance increases, the number of cells that develop EADs increases in the independent series. Conversely, for the co-expression models, there are no EADs even at variances up to 0.4. **C.** Variance of the APD_{90} distributions for each set of conductance scalar inputs for independent (blue) and co-expression (red) of I_{Kr} and I_{CaL}. Note that the variance of the APD_{90} distribution was always greater for the independent simulations ($p<0.008$ between groups, paired t-test)

Figure 4 Movie supplement 1

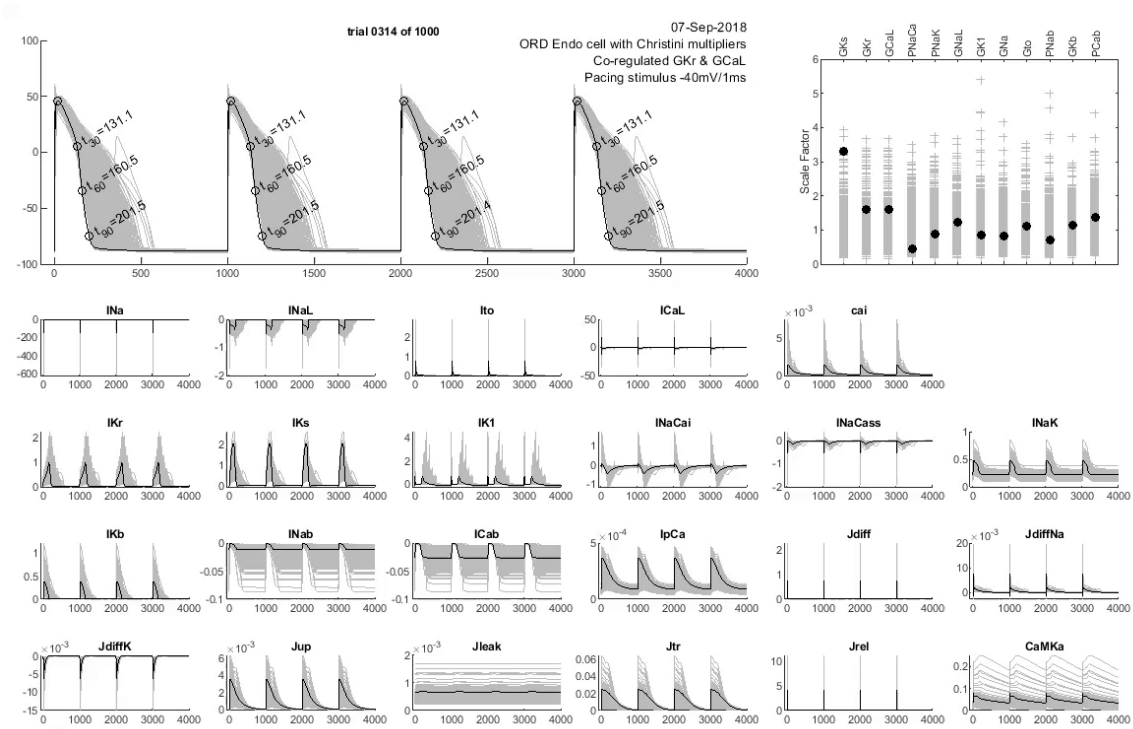

APD$_{90}$ values for both independent and co-expression cell populations becomes broader as the level of variability is increased (**Figure 4A-C**). However, the spread of APD$_{90}$ values in the cells with identical G_{CaL}-G_{Kr} scalars is always narrower than in the cell populations with independent G_{CaL}-G_{Kr} scalar values. For example, in the case of **Figure 4B,** the variance of the APD$_{90}$ values was 0.026 for the co-expression dataset but 0.046 for the independent dataset (see **Figure 4 figure supplement 1**). Another notable feature of the data in **Figure 4C** is that early afterdepolarizations (EADs) begin to appear in the cell population with independent scalars when the scalar variability, σ^2, exceeds 0.20 (also see **Figure 4 Figure supplement 1**). The number of cells with an EAD are indicated in parentheses above each distribution in **Figure 4C.**

We next investigated whether coupling of the conductance scalars for G_{Kr} and G_{CaL} influenced the generation of EADs in response to a pathological stimulus. Specifically, we investigated how cells respond to drug block of I_{Kr} which is the underlying cause of di-LQTS (22). Populations of action potentials obtained for independent and co-expression

populations with I_{Kr} block of 0%, 50% and 80% are illustrated in **Figure 5**. As the extent of I_{Kr} block is increased (from A to C), the proportion of action potentials producing EADs increases. It is also clear that at lower levels of I_{Kr} block, EADs were more frequent when G_{CaL} and G_{Kr} scalars were modulated independently (see **Figure 5B** and inset to **Figure 5D**). However, the proportion of simulations developing EADs in both the independent and co-expression populations becomes similar when the extent of I_{Kr} block exceeds 80% (**Figure 5D**).

It is well established that the extent of repolarization prolongation seen in patients prescribed drugs that block I_{Kr} is highly variable and only a subset of patients exposed to drugs that block I_{Kr} (29), or with a mutation causing 50% loss of I_{Kr} function (30), will develop life threatening

Figure 5: Impact of G_{Kr}-G_{CaL} co-expression on response to drug block of I_{Kr}

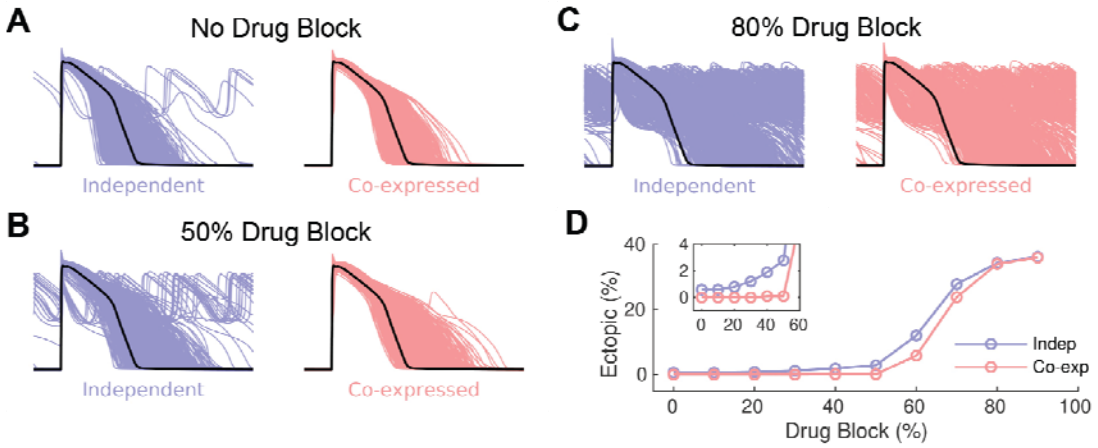

APs for co-expressed G_{Kr}-G_{CaL} (red) and independent (blue) G_{Kr}-G_{CaL} populations, with scalar variance $\sigma^2 = 0.25$, for **A.** control, **B.** 50% I_{Kr} block and **C.** 80% I_{Kr} block. **D.** plot of % of AP simulations with EADs versus % I_{Kr} block (co-expression, red and independent, blue). The inset in panel D shows an expanded view of the % EADs at small levels of I_{Kr} block.

arrhythmias. This is consistent with the prediction made by our simulated drug block experiments shown in **Figure 5**. We therefore asked whether the data from the co-expression datasets could tell us anything about what factors might predispose to lesser or greater extent of AP prolongation and/or the development of EADs in the presence of a drug that blocks I_{Kr}. Analysis of the subset of scalars within the co-expression dataset that

354 produced the 50 longest APs without EADs, compared to the subset of scalars that resulted
355 in APs with EADs, is illustrated in **Figure 6A and 6B** respectively. Notably, the longest APs
356 without EADs had low G_{CaL} scalars (and hence low G_{Kr} scalars before addition of drug
357 block). Conversely, the APs that developed EADs had higher G_{CaL} and G_{Kr} scalars. In **Figure**
358 **6C**, we have plotted the APD_{90} values for cells in the highest (red) and lowest (blue)
359 quartiles of G_{Cal} - G_{Kr} scalars. As expected, the low G_{CaL} group showed longer APD_{90} values
360 on average compared to the high G_{CaL} group (see the continuous lines in **Figure 6C**).
361 Furthermore, for the 70% I_{Kr} block scenario, 44% of the high G_{CaL} group have developed
362 EADs whereas only 7% of the low G_{CaL} group have developed EADs (compare red and blue
363 bars at 70% drug block in **Figure 6C**). Thus, higher G_{CaL} is associated with a greater risk of
364 developing EADs in response to moderate levels of I_{Kr} block. A similar pattern of results
365 was observed when G_{CaL} and G_{Kr} were allowed to vary independently, except that in this
366 scenario the difference between the high G_{CaL} and low G_{CaL} groups was even more dramatic
367 at lower levels of I_{Kr} block (see **Figure 6, figure supplement 1**).

368 A corollary of our prediction that patients with high G_{CaL} are more susceptible to EADs
369 when exposed to a drug that blocks I_{Kr}, is that co-administration of a drug that blocks I_{CaL}
370 would reduce the incidence of EADs. Magnesium, which is used in the acute management
371 of di-LQTS (14), is a weak calcium channel blocker. Raising plasma [Mg^{2+}] from 1.5 to 2.5
372 mM would be expected to inhibit I_{CaL} by ~20% (31), conversely reducing [Mg^{2+}] from 1.5
373 to 0.5 mM would be expected to increase I_{CaL} by ~20%. When we increased I_{CaL} by 20%,
374 the incidence of EADs in the high G_{CaL} group increased from 10% to 16% for the 60% I_{Kr}
375 block simulation and from 44% to 58% for the 70% I_{Kr} block simulations (see **Figure 7)**. A
376 drug that inhibited I_{CaL} by 20% caused a modest decrease in the percentage of cells with
377 EADs and reduction of I_{CaL} by 50% had a correspondingly larger effect, for example,
378 reducing EADs from 44% to 12% in the 70% I_{Kr} block scenario (**Figure 7**).
379

Figure 6: High G_{CaL} increases risk of EAD formation at moderate I_{Kr} block

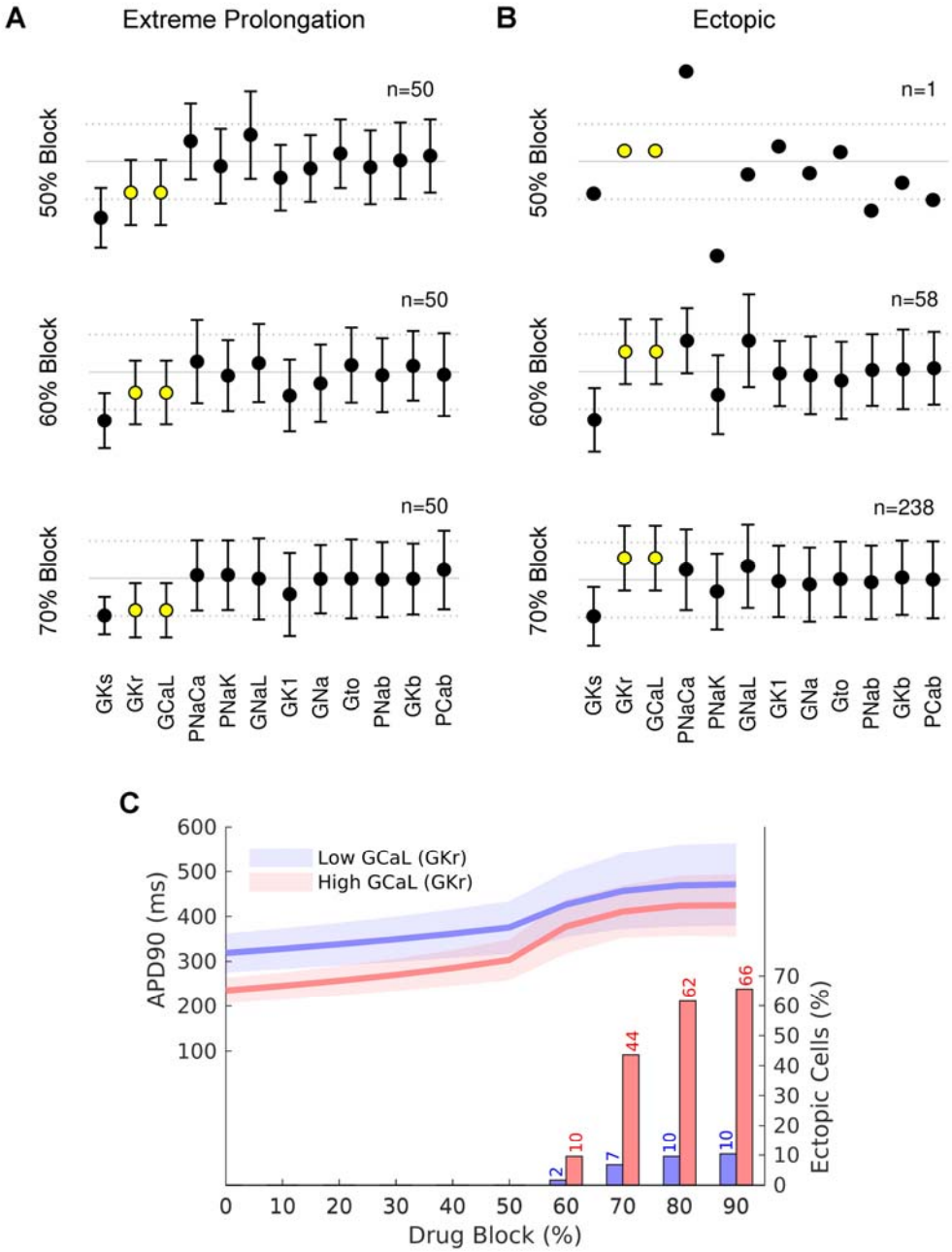

Scalars (mean ± SD) for the population of cells with G_{Kr}-G_{CaL} co-expression. **A.** 50 cells with the longest APD_{90} values and no EAD with increasing % I_{Kr} block. **B.** Scalars (box and whisker plots) for cells with EADs with increasing % I_{Kr} block. The G_{CaL} and G_{Kr} scalars are highlighted in yellow. **C.** APD_{90} values (left axis) for the highest (red) and lowest (blue) quartile of cells according to baseline G_{CaL} scalar. The continuous lines show the mean value and shaded area shows ±1 SD). The percentage of EADs in each quartile is shown as columns (see axis on right side of graph). The corresponding plots for the population of cells with independent G_{Kr}-G_{CaL} scalars are show in the **Figure 6 figure supplement 1.**

Figure 6: figure supplement 1: High G_{CaL} increases risk of EAD formation at moderate I_{Kr} block even when G_{CaL} and G_{Kr} are varied independently

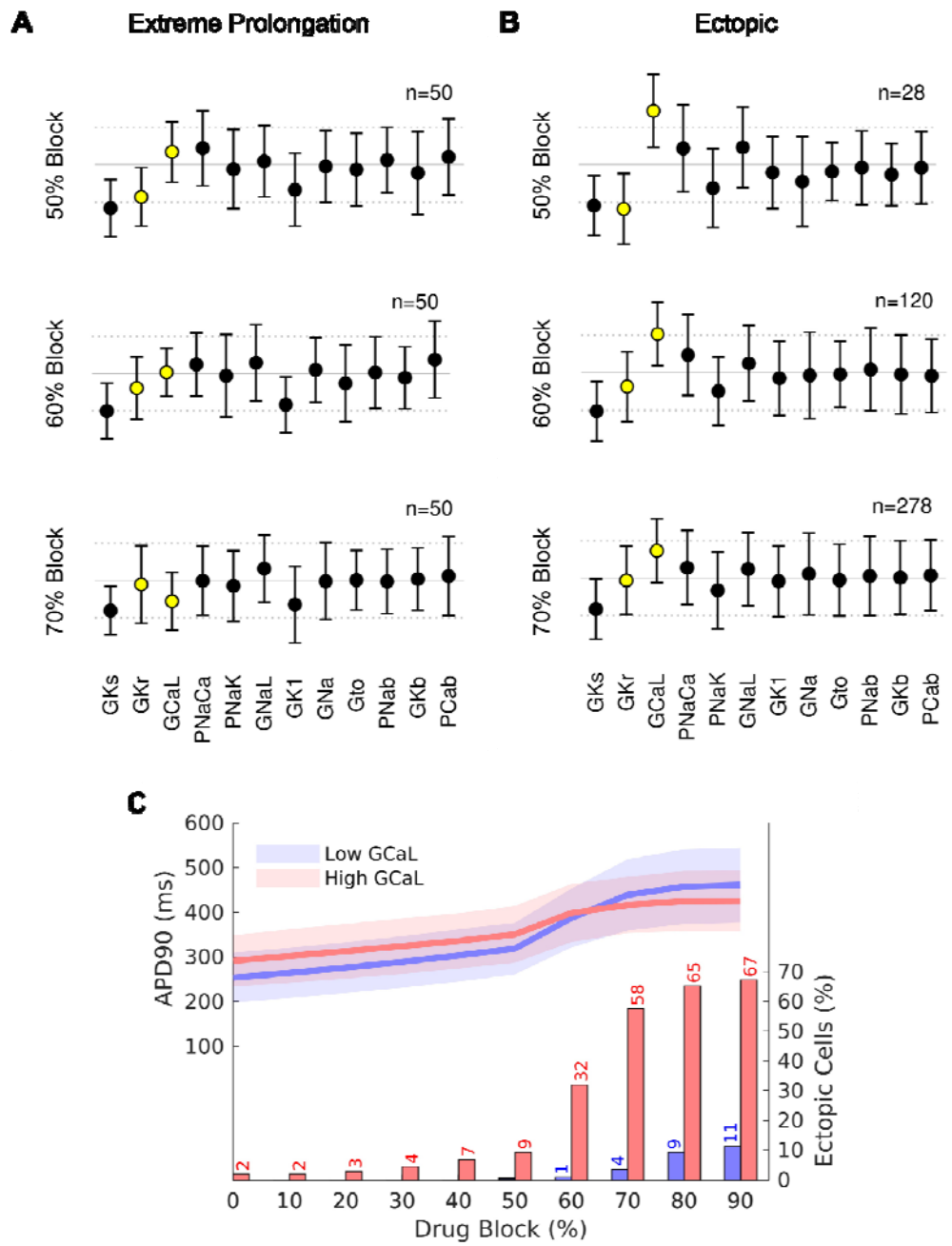

Conductance scalars (mean ± SD) that give **A**. The 50 most extreme APD values or **B**. EADs for the population of cells with independent regulation of G_{Kr} and G_{CaL}. **C**. Plot of APD_{90} values for the highest quartile of G_{CaL} (red) and lowest quartile of G_{CaL} (blue) versus % drug block of I_{Kr}. The continuous line shows mean and shaded regions show ± 1 standard deviation. The column graph shows the % of cells that develop EADs at each level of drug block.

Figure 7: Effect of modifying I_{CaL} on incidence of EADs in response to I_{Kr} drug block.

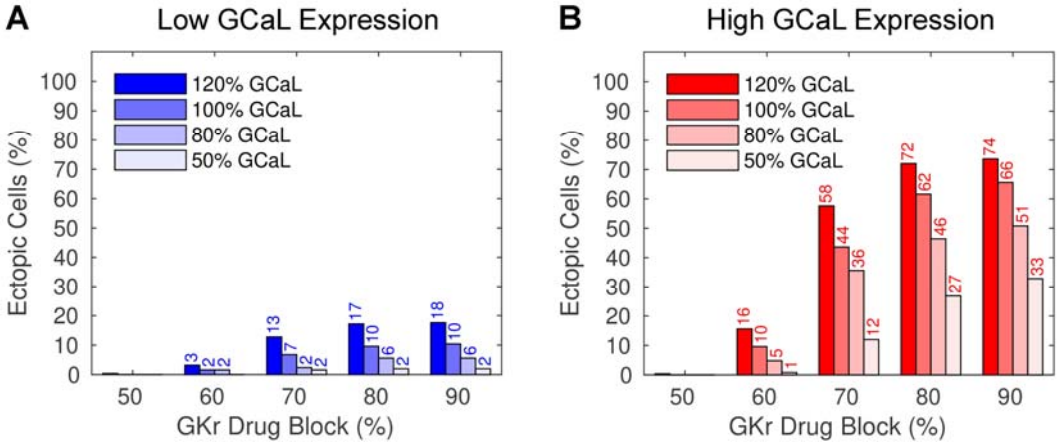

I_{CaL} was increased 20% to mimic hypomagnesaemia, reduced 20% to mimic hypermagnesaemia (see text for details), or reduced 50% to mimic administration of a calcium channel blocker. In both the quartile of cells with the lowest G_{CaL} scalars (blue, **A**) and the quartile of cells with the highest G_{CaL} scalars (red, **B**) the incidence of EADs increased when G_{CaL} was enhanced and decreased when G_{CaL} was decreased. The observed differences were most pronounced with moderate (60-70%) I_{Kr} drug block.

To determine whether our *in silico* predictions could be validated in cardiac myocytes we investigated whether the extent of I_{Kr}-block induced prolongation of repolarization seen in cardiac myocytes derived from different hiPSC lines were correlated with the levels of *KCNH2* gene expression. We measured the duration of repolarization from extracellular field potentials (FPD) recorded from monolayers of hiPSC-derived cardiac myocytes paced at 1 Hz (see **Figure 8**). Cisapride (200 nM), a highly selective I_{Kr} blocker (32), caused a prolongation of repolarization that varied between 17.9 ± 7.4 ms (mean ± SD, n=12) for the least sensitive cell line to 98 ± 41 ms (mean ± SD, n=11) for the most sensitive cell line (**Figure 8A**). There was a significant inverse correlation between the extent of FPD prolongation and the [*KCNH2*-mRNA] measured for each cell line (**Figure 8B**). Furthermore, the extent of FPD prolongation caused by Cisapride in each cell line was almost exactly reversed by Nifedipine (50 nM), a highly selective I_{CaL} blocker (32) (Figure 8A).

Figure 8: Effect of I_{Kr} and I_{CaL} inhibition on repolarization duration in iPSC-CM

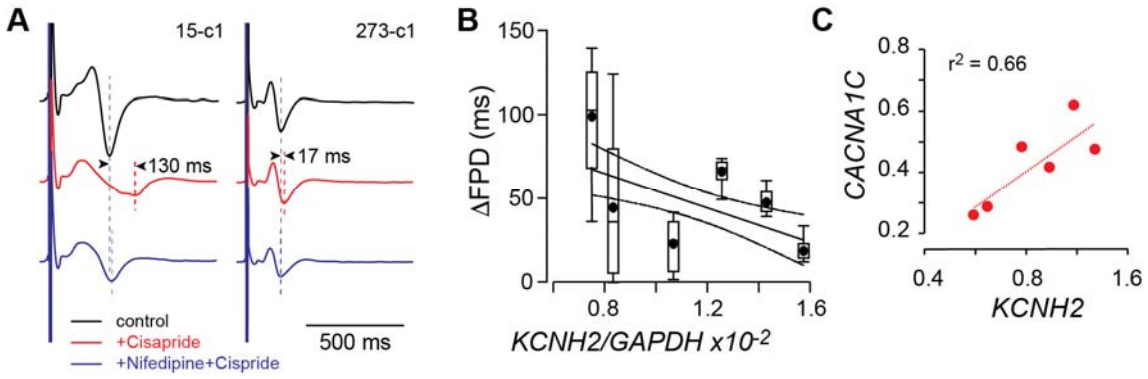

A. Example extracellular electrograms recorded from two separate hiPSC-CM lines under control (black) conditions, after 5 minutes perfusion with cisparide (200 nM, red)followed by 5 minutes perfusion with cisapride (200 nM) + nifedipine (50 nM, blue). In cell line 15-c1 there was a 130 ms prolongation in field potential duration (FPD) which almost completely reversed on addition of nifedipine. In cell line 273-c1 there was a much smaller prolongation of 17 ms with addition of Cisapride that again reversed on the addition of Nifedipine. **B**. Summary of ΔFPD for 6 cell lines plotted against the level of *KCNH2* mRNA (normalised to GAPDH expression). Data shown as box and whiskers (median, box: 25%-75%, extremities: 5%-95% with the mean shown as a filled circle, n=7-12 replicates for each cell line). The straight line of best fit is shown as a solid line with 95% confidence intervals shown as dashed lines; the slope of the line is significantly different to zero (F-test, p=0.0010). The micro-electrode array data for panels A&B are provided in Figure 8 -Source Data 1. **C**. Plot of normalised mRNA expression for *KCNH2* versus *CACNA1C* for the cell lines used in the experiments summarized in panel B. To account for any differences in mRNA loading between runs, levels of expression have been normalized to GAPDH. The mRNA data for panels B&C are provided in Figure 8 -Source Data 2 (GEO: TBA).

Discussion

Cardiac electrical activity is regulated by the interdependent activity of a plethora of ion channels, transporters and calcium handling proteins (4). Understanding the precise details of how these conductances interact to control the rhythm of the heart has been an enduring source of fascination. In this study, we have used meta-analytical techniques to interrogate the large numbers of RNASeq datasets that have been deposited in public

507 access databases, to look for patterns of co-expressed genes that might help decipher the
508 control of cardiac electrical activity. The most important pair of co-expressed genes,
509 identified both in the public RNA Seq datasets (**Figure 1**) and in heart cells derived from
510 hiPSC lines (**Figure 2**), was that of *CACNA1C* (I_{CaL}) and *KCNH2* (I_{Kr}). Using an *in silico*
511 approach we demonstrated that tight co-expression of *CACNA1C* and *KCNH2*, against a
512 background of variability of all other ion channels, helps to control the duration of
513 repolarization (**Figure 4**). More importantly, the co-expression of *CACNA1C* and *KCNH2*
514 helps to protect the heart from early after depolarizations when they are exposed to drugs
515 that block I_{Kr} (**Figure 5**). Our simulations also suggest that inter-individual differences in
516 pro-arrhythmic responses to I_{Kr} drug block can be explained by inter-individual
517 differences in levels of *CACNA1C* expression (**Figure 6**). Finally, our *in vitro* experiments
518 on cardiac myocytes derived from hiPSC lines confirmed that the extent of repolarization
519 prolongation seen with block of I_{Kr} was inversely correlated with the level of *KCNH2* mRNA
520 expression (**Figure 8**) and the tight correlation between I_{Kr} block-induced FPD
521 prolongation and I_{CaL} block-induced repolarization shortening validates the tight coupling
522 between I_{Kr} and I_{CaL} expression despite marked differences in the absolute levels of
523 expression between different cell lines.

524 Over the last few years, numerous groups have shown that there is considerable
525 heterogeneity of ion channel expression amongst excitable cells, including neurons (33)
526 and cardiac myocytes (7,19). Furthermore, since the pioneering work of Eva Marder and
527 colleagues, the presence of modules of co-expressed ion channel genes has also been well
528 appreciated (15). These previous studies, however, relied on patch clamp analysis of
529 isolated cells (15,34) and qPCR analysis (15) or single molecule fluorescence *in situ*
530 hybridization (35) of individual ion channel mRNAs, which are highly laborious techniques
531 and so have been restricted to only a few important ion channel genes. The advent of high
532 throughput transcriptomic analyses has greatly facilitated the identification of conserved
533 networks of co-expressed gene modules amongst the entire set of expressed genes (21).
534 By applying meta-analytic approaches to a large number of independent datasets one can
535 more readily discern genuine co-expression signals from noise, as well as explore smaller
536 gene modules (21). In our analysis of a subset of rhythmonome genes within a large

537 library of public RNA Seq datasets, we identified two clusters of genes: a first subset that
538 predominantly affects calcium handling and a second subset that predominantly affects
539 membrane potential (see **Figure 1**). The nodes within each of these clusters that are most
540 closely connected within the rhythmonome relative to all other genes are *KCNH2* and
541 *CACNA1C* (see **Figure 1 figure supplement 1**). This is analogous to a network of networks
542 (36), where the *KCNH2-CACNA1C* link provides an interconnection of the two networks.
543 Independent evidence to corroborate an important link between calcium handling and
544 regulation of cardiac action potential duration comes from the large genome-wide
545 association studies (GWAS) of QT interval duration which identified SNPs in a number of
546 calcium handling genes as well as *KCNH2* as being important determinants of QT interval
547 in the population (37).

548 Due to the large number of associations we were testing for in our network analyses, it is
549 possible that some would occur by chance. That we were able to confirm the presence of at
550 least some of the co-expression modules in an independent dataset, i.e. the hiPSC-CM (see
551 **Figure 2**) provides important corroborative evidence that these co-expression patterns
552 are real and therefore likely to have physiological relevance. It should also be noted that
553 many ion channels important for function in adult cardiac myocytes are not expressed at
554 significant levels in immature cardiac myocytes, such as those derived from hiPSC (e.g.
555 *SCN5A*, *KCNQ1*, *KCNJ12*, *KCND3*, (26)). It is therefore possible that we have underestimated
556 the number of genes within the modules of co-expressed genes in adult cardiac myocytes.

557 The patterns of co-expressed genes we observed show some important similarities, as well
558 as differences to previous studies. Banyasz et al. (34) and Rees et al. (18) have both
559 demonstrated that the expression of I_{CaL} is correlated with the sum of the major
560 repolarizing ion currents in guinea-pig and mouse respectively. However, the molecular
561 players involved in cardiac electrical activity in rodents are quite distinct to humans (38).
562 In humans, the most important determinant of repolarization duration at baseline is I_{Kr}
563 (39), whereas in guinea-pig I_{Ks} and I_{Kr} play equally important roles (34) and in mice the
564 fast component of the transient outward current ($I_{to,f}$) and the ultra-rapid delayed rectifier
565 (I_{Kur}) are the major repolarization currents (18). Thus, there is a common factor between
566 our study showing co-expression of *KCNH2* and *CACNA1C* in human and the previous

567 rodent studies, i.e., all studies show a correlation between I_{CaL} and the major repolarizing
568 currents present in that species. Our study, however, is the first to demonstrate the
569 importance of co-expressed genes in human heart tissue. In addition to co-regulation at
570 the level of gene expression, there is also evidence for co-ordinated regulation of modules
571 of ion channels occurring at post-transcriptional levels (35,40). That we still observe an
572 inverse correlation between *KCNH2* mRNA levels and repolarization duration in hiPSC-
573 derived cardiac myocytes, as predicted from our *in silic*o analyses, demonstrates that co-
574 regulation at the level of gene expression is still an important determinant of overall
575 cardiac electrical function.

576 Identifying modules of co-expressed genes are the first step in seeking to understand the
577 logic of complex systems (6). Understanding how such modules impact function in health
578 and disease is the next challenge. In neuronal cells, Marder and colleagues have shown
579 that modules of co-expressed ion channels play an important role in regulating action
580 potential firing patterns (41). Rees and colleagues, have demonstrated that modules of co-
581 expressed depolarization and repolarization currents can help to ensure normal amplitude
582 calcium transients, a critical determinant of overall heart function (18). We have extended
583 these studies to show that in normal heart cells, co-expression of *KCNH2* (repolarization)
584 and *CACNA1C* (depolarization) channels help to maintain the plateau duration of the action
585 potential, which in turn likely contributes to regulating the duration and amplitude of the
586 calcium transient. More importantly, our studies provide the first insights into how
587 patterns of co-expressed ion channel genes influence the hearts response to pathological
588 stimuli.

589 Sudden death due to abnormalities of cardiac electrical signaling is a major cause of
590 mortality (1). Predicting in advance who is more or less susceptible to sudden cardiac
591 death and therefore warrants prophylactic treatment remains challenging (2). A key to
592 being able to predict who is at greatest risk is understanding why different people respond
593 differently to the same pro-arrhythmic stimulus. Based on the results of our *in silico*
594 studies, validated by *in vitro* analyses of hiPSC-derived cardiac myocytes, we have
595 provided two important insights into the nature of interindividual risk for developing
596 arrhythmias in response to drugs that block I_{Kr}, the major cause of drug-induced cardiac

597 arrhythmias (14). First, cells with low G_{CaL} (and hence low G_{Kr} at baseline) exhibited the
598 greatest prolongation of AP duration when exposed to I_{Kr} drug block. Second, cells with
599 high G_{CaL} (and hence high G_{Kr} at baseline) showed greater propensity for development of
600 EADs at moderate levels of I_{Kr} drug-block (**Figure 6**). An important implication of the
601 observation that a high G_{CaL} increases the susceptibility to EADs in response to drug block
602 of I_{Kr} is that the co-administration of an I_{CaL} blocker should reduce the risk of EADs (as
603 shown in **Figure 7**). This is consistent with the observation that the administration of
604 magnesium, which is a mild calcium channel blocker (31), is helpful in the acute
605 management of patients with drug-induced *torsades de pointes* (14), and conversely that
606 hypomagnesaemia, which would stimulate I_{CaL}, can exacerbate *torsades de pointes* (42). It
607 is also consistent with the observation that drugs that block I_{CaL} and I_{Kr} (e.g., verapamil)
608 are not associated with drug-induced arrhythmias (43) and that verapamil prevented the
609 development of *torsades de pointes* in rabbit hearts exposed to an I_{Kr} blocker (44).
610 However, given that calcium channel blockers are contra-indicated in some ventricular
611 arrhythmias (45), and the likelihood that patients who have drug-induced LQTS may have
612 other underlying cardiac conditions (14), one should be cautious about prescribing
613 calcium channel blockers. Conversely, it would be reasonable to consider using calcium
614 channel blockers to treat patients with LQTS type 2 (i.e. patients with an isolated loss of I_{Kr}
615 function) who continue to have cardiac events despite treatment with ß-blockers (46).

616 In summary, we have demonstrated that meta-analysis of large-scale gene expression data
617 sets is a powerful technique for discerning underlying patterns in gene expression, and
618 that this can provide insights into disease causation at an individual level. Specifically, we
619 have demonstrated that the co-expression of *KCNH2* (I_{Kr}) and *CACNA1C* (I_{CaL}) plays an
620 important role in regulating cardiac repolarization both in health and in disease.

621

622 **Methods**

623 **Analysis of public RNASeq datasets**

624 An aggregate co-expression gene network was built from public data, similar to that
625 described previously (47). Briefly, 75 human RNA-seq expression experiments (listed in

626 **Figure 1 source data 1**) that passed quality control and had a least 10 samples (3653
627 samples in total) were downloaded from the Gemma database (48). Approximately thirty
628 thousand genes were used for the network, limited only to those with Entrez gene
629 identifiers. A co-expression network was generated for each experiment by calculating
630 Spearman's correlation coefficients between every gene pair and then ranking these
631 values (47). An aggregate gene co-expression network was then generated by averaging
632 across all the individual networks, and re-ranking the final network. This final aggregate
633 network was then used to determine the co-expression ranking between genes that
634 encode for the set of ion channels and calcium handling proteins that determine the shape
635 and duration of the human ventricular AP, the so-called rhythmonome gene subset (see
636 **Figure 1 source data 1**). Network connectivity of the gene set was measured by
637 comparing the weighted local node degree to the global node degree (49). Node degrees
638 are the sum of the total connections a node (here gene) has within a network. Local node
639 degree refers to the sum of connections (here the ranked correlation) within the
640 rhythmonome gene set, while global node degree is the sum of connections to that gene
641 across all the genes in the network. Code for the analysis is available at
642 https://github.com/sarbal/hERG-cal

643

644 **Human induced pluripotent stem cell derived cardiac myocytes.**

645 Human iPSC lines, generated from healthy patients by Stanford Cardiovascular Institute
646 Biobank, as previously described (50), were a generous donation from Joseph Wu
647 (Standford Cardiovascular Institute). HiPSC colonies were maintained on Matrigel®
648 (Corning) coated plates in chemically defined medium (mTeSR1™, StemCell technologies),
649 and passaged using Dispase (StemCell technologies). For differentiation, hiPSCs were
650 dissociated by incubating at 37°C for 7 minutes with TrypLE™ Express (ThermoFisher)
651 and seeded at 125000 cells/cm^2 on a Matrigel® coated 12 well plate, in mTeSR™1 medium
652 supplemented with StemMACS™ Y27632 (Miltenyi Biotec). Once the cells reached greater
653 than 95% confluency, differentiation was initiated using STEMdiff™ Cardiomyocyte (CM)
654 differentiation and Maintenance Kit (StemCell technologies). At day 15, CMs were
655 dissociated by incubation in Collagenase Type I (ThermoFisher) for 45 minutes at 37°C to

656 break up the matrix and then incubated in 0.25% Trypsin with EDTA for 7 minutes at
657 room temperature followed by filtering through a 40 μm cell strainer (51). The CMs were
658 seeded on a Matrigel coated 96-well plate (Greiner Bio-One) and maintained in CM
659 maintenance medium for 10-15 days before they were harvested for mRNA expression
660 analysis. Total RNA was obtained from 40,000 hiPSC-CMs lysed using QIAzol Lysis reagent
661 (Qiagen). The RNA was purified using miRNeasy® Mini Kit (Qiagen), and all samples had
662 RIN values >7.5, and were analysed using Agilent Bioanalyzer pico-chip. RNA samples
663 were hybridised with probes designed to detect 35 known rhythmonome genes using
664 nCounter (NanoString Technologies, see **Figure 2 source data 1**), which was performed at
665 the Ramaciotti Centre for Genomics (UNSW). For quantitative comparisons of different
666 mRNA species across different runs we normalised mRNA levels, relative to GAPDH, to
667 account for any variation in mRNA loading levels. Raw data for mRNA expression levels
668 are provided Figure 2 -Source Data 1 and Figure 8 -Source Data 2

669 Extracellular field potentials were recorded from hiPSC-CM monolayers using a Maestro-
670 APEX multi-electrode array (MEA) system (Axion Biosystems, Atlanta, GA, USA) as
671 previously described (52). Briefly, cell monolayers were maintained for 20-30 days in
672 STEMDiff cardiomyocte maintenance media (STEM CELL Technologies), on EStim classic
673 48 well MEA plates (Axion Biosystems, Atlanta, USA), prior to recording. Monolayers,
674 maintained at 37°C, were paced at 1 Hz and signals digitized at 12.5 kHz using AxIS
675 v2.5.1.10 software (Axion Biosystems, Atlanta, GA, USA). Field potential durations were
676 measured from the peak depolarization spike to the peak of the repolarization wave. After
677 30 minutes of pacing equilibration, Electrograms were recorded for 5 minutes in control
678 conditions, 5 minutes in the presence of cisapride (200nM), and for 5 minutes in the
679 presence of cisparide + nifedipine (50 nM) and measurements averaged over the last 10
680 beats of each recording period. This allowed for the possibility that if there was any beat to
681 beat variation this could be averaged out over the ten beats. Twelve wells were plated for
682 each line and all wells from which signals were recorded (n=7-12) were included in the
683 analysis. After the MEA recordings were completed cells were harvested for mRNA
684 analysis, as described above. Raw data for MEA recordings are provided in Figure 8 -
685 Source Data 1.

Computer modelling

Human cardiac APs were simulated using the endocardial configuration of the O'Hara-Rudy (ORD11) model (27) with key conductances modified as described by Krogh-Madsen et al. (28). The original ORD11 code was adapted to run in the Brain Dynamics Toolbox for Matlab (53). To incorporate population variability in ion channel expression levels the maximum conductance for each current was multiplied by conductance scalar (G_x), that was drawn from a random log-normal distribution (39), with unit mean and variance that was systematically manipulated from 0.05 to 0.5. All models were paced at 1Hz with a stimulus of -40 mV and duration of 1 ms and allowed to equilibrate for 300 beats. We then analysed the next four beats (to allow for the possibility of development of alternans) after the equilibration stage. The peaks in those APs were identified using the Matlab *findpeaks* function. Individual beats were classified as ectopic if they had secondary peaks that were separated by more than 100 ms. The set of four beats were further classified as *alternans* if the profile of any of the APs deviated from each other by more than 1 mV at any time point. In a second set of simulations, we repeated the same method as above except that the random multipliers applied to both I_{CaL} and I_{Kr} were identical. This case we denote co-expression whereas the former case we denote independent expression. Code for the AP modeling is available at https://git.victorchang.edu.au/projects/CC/repos/ordcoreg.

Acknowledgements

This work was supported by the Victor Chang Cardiac Research Institute Innovation Centre, funded by the NSW Government. We also thank Terry Campbell, Dan Roden and Raj Subbiah for helpful discussions.

Funding

714 This work was supported by grants from the National Health and Medical Research
715 Council (NHMRC), App1116948 (to JIV), App1074386 (to JIV), App1164518 (to APH), and
716 from the National Institutes of Health (NIH) R01LM012736 (to JAG), R01MH113005 (to
717 JAG).
718

719 **References**

720

721 1. Zipes DP, Wellens HJ. Sudden cardiac death. Circulation. 1998;98(21):2334–51.

722 2. Behr E, Ensam B. New approaches to predicting the risk of sudden death. Clinical
723 Medicine. 2016;16(3):283–3.

724 3. Jan LY, Jan YN. Voltage-gated potassium channels and the diversity of electrical
725 signalling. J Physiol (Lond). 2012;590(11):2591–9.

726 4. Noble D, Garny A, Noble PJ. How the Hodgkin-Huxley equations inspired the Cardiac
727 Physiome Project. J Physiol (Lond). 2012;590(11):2613–28.

728 5. Marder E, Goaillard J-M. Variability, compensation and homeostasis in neuron and
729 network function. Nat Rev Neurosci. 2006;7(7):563–74.

730 6. Weiss JN, Karma A, MacLellan WR, Deng M, Rau CD, Rees CM, et al. "Good enough
731 solutions" and the genetics of complex diseases. Circ Res. 2012;111(4):493–504.

732 7. Prinz AA, Billimoria CP, Marder E. Alternative to Hand-Tuning Conductance-Based
733 Models: Construction and Analysis of Databases of Model Neurons. J Neurophysiol.
734 2003;90(6):3998–4015.

735 8. Britton OJ, Bueno-Orovio A, Van Ammel K, Lu HR, Towart R, Gallacher DJ, et al.
736 Experimentally calibrated population of models predicts and explains intersubject
737 variability in cardiac cellular electrophysiology. Proceedings of the National
738 Academy of Sciences. 2013;110(23):E2098–105.

739 9. Sarkar AX, Sobie EA. Quantification of repolarization reserve to understand inter-
740 patient variability in the response to pro-arrhythmic drugs: a computational
741 analysis. Heart Rhythm 2011;8(11):1749–55.

742 10. Liberos A, Bueno-Orovio A, Rodrigo M, Ravens U, Hernandez-Romero I, Fernandez-
743 Aviles F, et al. Balance between sodium and calcium currents underlying chronic
744 atrial fibrillation termination_ An in silico intersubject variability study. Heart
745 Rhythm. 2016;13(12):2358–65.

746 11. Passini E, Mincholé A, Coppini R, Cerbai E, Rodríguez B, Severi S, et al. Mechanisms
747 of pro-arrhythmic abnormalities in ventricular repolarisation and anti-arrhythmic
748 therapies in human hypertrophic cardiomyopathy. J Mol Cell Cardiol.
749 2016;96(C):72–81.

750 12. Marder E. Understanding Brains: Details, Intuition, and Big Data. PLoS Biol.
751 2015;13(5):e1002147–6.

752 13. O'Leary T, Sutton AC, Marder E. Computational models in the age of large datasets.
753 Curr Opin Neurobiol. 2015;32:87–94.

754 14. Roden DM. Drug-induced prolongation of the QT interval. N Engl J Med.
755 2004;350(10):1013–22.

756 15. Schulz DJ, Goaillard J-M, Marder EE. Quantitative expression profiling of identified
757 neurons reveals cell-specific constraints on highly variable levels of gene expression.
758 Proceedings of the National Academy of Sciences. 2007;104(32):13187–91.

759 16. Eisen MB, Spellman PT, Brown PO, Botstein D. Cluster analysis and display of
760 genome-wide expression patterns. Proceedings of the National Academy of Sciences.
761 1998 95(25):14863–8.

762 17. Gaiteri C, Ding Y, French B, Tseng GC, Sibille E. Beyond modules and hubs: the
763 potential of gene coexpression networks for investigating molecular mechanisms of
764 complex brain disorders. Genes Brain Behav. 2013;13(1):13–24.

765 18. Rees CM, Yang J-H, Santolini M, Lusis AJ, Weiss JN, Karma A. The Ca2+ transient as a
766 feedback sensor controlling cardiomyocyte ionic conductances in mouse
767 populations. eLife. 2018;7:4417.

768 19. Lee HK, Hsu AK, Sajdak J, Qin J, Pavlidis P. Coexpression analysis of human genes
769 across many microarray data sets. Genome Res. 2004;14(6):1085–94.

770 20. Gillis J, Pavlidis P. The role of indirect connections in gene networks in predicting
771 function. Bioinformatics. 2011;27(13):1860–6.

772 21. Ballouz S, Verleyen W, Gillis J. Guidance for RNA-seq co-expression network
773 construction and analysis: safety in numbers. Bioinformatics. 2015;31(13):2123–30.

774 22. Vandenberg JI, Walker BD, Campbell TJ. HERG K+ channels: friend and foe. Trends
775 Pharmacol Sci. 2001;22(5):240–6.

776 23. Bush WS, Crawford DC, Alexander C, George AL Jr, Roden DM, Ritchie MD. Genetic
777 variation in the rhythmonome: ethnic variation and haplotype structure in
778 candidate genes for arrhythmias. Pharmacogenomics. 2009;10(6):1043–53.

779 24. Sah R, Ramirez RJ, Backx PH. Modulation of Ca 2+Release in Cardiac Myocytes by
780 Changes in Repolarization Rate. Circ Res. 2002;90(2):165–73.

781 25. Sayed N, Liu C, Wu JC. Translation of Human-Induced Pluripotent Stem Cells. J Am
782 Coll Cardiol. 2016;67(18):2161–76.

783 26. Robertson C, Tran DD, George SC. Concise Review: Maturation Phases of Human
784 Pluripotent Stem Cell-Derived Cardiomyocytes. Stem Cells 2013;31(5):829–37.

785 27. O'hara T, Virág L, Varró A, Rudy Y. Simulation of the Undiseased Human Cardiac
786 Ventricular Action Potential: Model Formulation and Experimental Validation. PLoS
787 Comput Biol. 2011;7(5):e1002061–29.

788 28. Krogh-Madsen T, Jacobson AF, Ortega FA, Christini DJ. Global Optimization of
789 Ventricular Myocyte Model to Multi-Variable Objective Improves Predictions of
790 Drug-Induced Torsades de Pointes. Frontiers in Physiology. 2017;8:e1000173–10.

791 29. Pedersen HS, Elming H, Seibæk M, Burchardt H, Brendorp B, Torp-Pedersen C, et al.
792 Risk Factors and Predictors of Torsade de Pointes Ventricular Tachycardia in
793 Patients With Left Ventricular Systolic Dysfunction Receiving Dofetilide. Am J
794 Cardiol. 2007;100(5):876–80.

795 30. Shimizu W, Moss AJ, Wilde AAM, Towbin JA, Ackerman MJ, January CT, et al.
796 Genotype-phenotype aspects of type 2 long QT syndrome. J Am Coll Cardiol.
797 2009;54(22):2052–62.

798 31. Hartzell HC. Effects of magnesium on inactivation of the voltage-gated calcium
799 current in cardiac myocytes. J Gen Physiol. 1989;94(4):745–67.

800 32. Harris K, Aylott M, Cui Y, Louttit JB, McMahon NC, Sridhar A. Comparison of
801 electrophysiological data from human-induced pluripotent stem cell-derived
802 cardiomyocytes to functional preclinical safety assays. Toxicol Sci. 2013;134(2):412-
803 26

804 33. Marder E, Goaillard J-M. Variability, compensation and homeostasis in neuron and
805 network function. Nat Rev Neurosci. 2006;7(7):563–74.

806 34. Bányász T, Horváth B, Jian Z, Izu LT, Chen-Izu Y. Sequential dissection of multiple
807 ionic currents in single cardiac myocytes under action potential-clamp. J Mol Cell
808 Cardiol 2011;50(3):578–81.

809 35. Eichel CA, Ríos-Pérez EB, Liu F, Jameson MB, Jones DK, Knickelbine JJ, Robertson GA.
810 A microtranslatome coordinately regulates sodium and potassium currents in the
811 human heart. Elife. 2019 Oct 31;8. pii: e52654

812 36. Min B, Zheng M. Correlated network of networks enhances robustness against
813 catastrophic failures. PLoS ONE. 2018;13(4):e0195539–13.

814 37. The QT Interval International GWAS Consortium (QT-IGC), Lundby A, Rossin EJ,
815 Steffensen AB, Acha MR, Newton-Cheh C, et al. Annotation of loci from genome-wide
816 association studies using tissue-specific quantitative interaction proteomics. Nat
817 Methods 2014;11(8):868–74.

818 38. Huang CL-H. Murine Electrophysiological Models of Cardiac Arrhythmogenesis.
819 Physiol Rev. 2017;97(1):283–409.

820 39. Sadrieh A, Mann SA, Subbiah RN, Domanski L, Taylor JA, Vandenberg JI, et al.
821 Quantifying the origins of population variability in cardiac electrical activity through
822 sensitivity analysis of the electrocardiogram. J Physiol (Lond) 2013;591(17):4207–
823 22.

824 40. Ponce-Balbuena D, Guerrero-Serna G, Valdivia CR, Caballero R, Diez-Guerra FJ,
825 Jiménez-Vázquez EN. Cardiac Kir2.1 and NaV1.5 Channels Traffic Together to the
826 Sarcolemma to Control Excitability. Circ Res. 2018;122(11):1501-1516

827 41. Marder E. Variability, compensation, and modulation in neurons and circuits.
828 Proceedings of the National Academy of Sciences. 2011;108(Supplement_3):15542–
829 8.

830 42. Roden DM, Iansmith DH. Effects of low potassium or magnesium concentrations on
831 isolated cardiac tissue. The American Journal of Medicine. 1987;82(3A):18–23.

832 43. Redfern WS, Carlsson L, Davis AS, Lynch WG, MacKenzie I, Palethorpe S, et al.
833 Relationships between preclinical cardiac electrophysiology, clinical QT interval
834 prolongation and torsade de pointes for a broad range of drugs: evidence for a
835 provisional safety margin in drug development. Cardiovasc Res. 2003;58(1):32–45.

836 44. Farkas AS, Makra P, Csík N, Orosz S, Shattock MJ, Fülöp F, et al. The role of the
837 Na+/Ca2+ exchanger, INa and ICaL in the genesis of dofetilide-induced torsades de
838 pointes in isolated, AV-blocked rabbit hearts. Br J Pharmacol. 2009;156(6):920–32.

839 45. Akhtar M, Tchou P, Jazayeri M. Use of calcium channel entry blockers in the
840 treatment of cardiac arrhythmias. Circulation 1989;80(6 Suppl):IV31–9.

841 46. Komiya N, Tanaka K, Doi Y, Fukae S, Nakao K, Isomoto S, et al. A patient with LQTS in
842 whom verapamil administration and permanent pacemaker implantation were
843 useful for preventing torsade de pointes. Pacing and Clinical Electrophysiology.
844 2004;27(1):123–4.

845 47. Ballouz S, Verleyen W, Gillis J. Guidance for RNA-seq co-expression network
846 construction and analysis: safety in numbers. Bioinformatics. 2015;31(13):2123–30.

847 48. Zoubarev A, Hamer KM, Keshav KD, McCarthy EL, Santos JRC, Van Rossum T, et al.
848 Gemma: a resource for the reuse, sharing and meta-analysis of expression profiling
849 data. Bioinformatics. 2012;28(17):2272–3.

850 49. Ballouz S, Gillis J. Strength of functional signature correlates with effect size in
851 autism. Genome Med. 2017;9(1):64.

50. Burridge PW, Diecke S, Matsa E, Sharma A, Wu H, Wu JC. Modeling Cardiovascular Diseases with Patient-Specific Human Pluripotent Stem Cell-Derived Cardiomyocytes. Methods Mol Biol.; 2016;1353(Chapter 196):119–30.

51. Mills RJ, Titmarsh DM, Koenig X, Parker BL, Ryall JG, Quaife-Ryan GA, et al. Functional screening in human cardiac organoids reveals a metabolic mechanism for cardiomyocyte cell cycle arrest. Proceedings of the National Academy of Sciences. 2017;114(40):E8372–81.

52. Perry MD, Ng CA, Mangala MM, Ng TYM, Hines AD, Liang W et al. Pharmacological activation of IKr in models of long QT Type 2 risks overcorrection of repolarization. Cardiovasc Res. 2019 Sep 13. pii: cvz247 (In Press)

53. Heitmann S, Aburn MJ, Breakspear M. The Brain Dynamics Toolbox for Matlab. Neurocomputing; 2018;315:82–8.

Supplementary Files

Figure 3 supplementary Movie 1: Simulations of 1000 APs with all conductance scalars allowed to vary independently

Figure 4 supplementary Movie 1: Simulations of 1000 APs with G_{Kr} and G_{CaL} scalars coupled but all other conductance scalars allowed to vary independently

Data Sets

Figure 1 – Source Data 1.xlsl

- Sheet 1: List of GEO datasets analysed
- Sheet 2: Co-expression rankings for rhythmonome genes
- Sheet 3: modules of co-expressed genes

Figure 2 – Source Data 1: nanostring datasets: GEO: TBA

- Sheet 1: Metadata
- Sheet 2: normalized mRNA read counts

Raw data files (uploaded to GEO)

Figure 8 – Source Data 1: Multi-electrode array datasets

1a: MEA guide.txt (description of contents of raw data files and how to extract the data).

1b: plate1_baseline.mat

1c: plate1_cis.mat

1d: plate1_nif.mat

1e: plate2_baseline.mat

1f: plate2_cis.mat

1g: plate2_nif.mat

Figure 8 – Source Data 2: nanostring datasets: GEO: TBA

Sheet 1: Metadata

Sheet 2: normalized mRNA read counts

Raw data files (uploaded to GEO)

Software Code

Figure 1,2; meta data analysis scripts: https://github.com/sarbal/hERG-cal

Figures 3-7: Baseline code and BD Toolbox software package used to generate figures 3-7: https://git.victorchang.edu.au/projects/CC/repos/ordcoreg.